Reaching Torque-Velocity Profiles of Human Muscles: The Adaptive Cycloidal Linear Drive

Cornelius Klas and Tamim Asfour, *Member, IEEE,*

***Abstract*—Building humanoid robots with properties similar to those of humans in terms of strength and agility is a great and unsolved challenge. In this work, we introduce an adaptive linear drive for fast and powerful motions in robotics with a light gear mechanism: The Adaptive Cycloidal Linear Drive (ACLD). The gear mechanism features two transmission ratios covering a nominal operation region ranging from fast low-torque motions to slow high-torque motions, with a speed-force profile similar to those of human muscles. This is contrary to the limited nominal operation region of electric motors with single-ratio gearboxes, and is realized by the new idea of adaptively combining a cycloidal stage with a linear spindle drive. The operation principle of the gear mechanism and hardware design of a prototype are described. Further, the properties of the prototype are measured and compared with state-of-the-art solutions in robot design as well as to the performance of human muscles.**

***Index Terms*—Mechanical design, reduction gearbox, transmission, gearshift, robotic actuator, humanoid robots.**

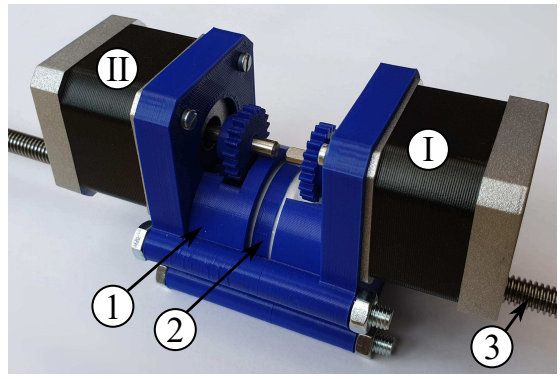

Fig. 1: Realization of the **ACLD** with stepper motors. All prototypes for this paper share the same gearbox size and design and differ only by motor type and spindle pitch. The components are marked according to Tab. II

I. Introduction

The challenge in the development of a humanoid robot lies in the combination of high-level functionality requirements and the highly complex mechatronic system consisting of drive trains, support structures and control systems that must be integrated into a limited installation space. For the realization of highly functional requirements, the gearboxes in the drive trains are one of the most important factors.

A suitable method for evaluating the capabilities of actuators is the use of their force-speed profile. This is the curve of the maximum force that an actuator provides at a given speed. For rotary actuators, this corresponds to the angular velocity-torque curve. The rectangular area ($force \cdot speed$) under a given point on the curve shows the mechanical power needed for this state.

Typically, electric motors deliver higher velocities and lower torques than the task requires, and a gearbox is added to increase torque whereby speed is reduced. Neglecting friction, a mechanical gearbox with a fixed transmission cannot change the shape of the motor speed-torque profile, the area under the curve or the maximal mechanical power. The gearboxes usually have independent, fixed limits for torque and speed, and the motors are selected and operated accordingly. If fixed limits for speed and torque are specified, the maximum mechanical power as a multiplication of the limits is high. Since many components get larger and heavier with the maximum power they have to withstand, this is often not the best solution.

Taking inspiration from nature, the force-speed profile of human muscles (Fig. 2) reaches the whole range with low maximum power. While the exact shape of this profile for different muscles is still under discussion, the general form is clear [1]: Low speed at high torque and high speed at low torque, with low peak power in the middle.

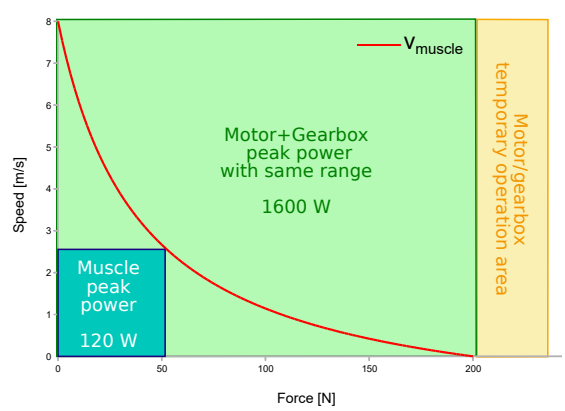

Fig. 2: Force and speed in muscles (biceps brachii from [2]) and an actuator with fixed speed and torque limits and the same range of speed and force.

This work has been supported by the Carl Zeiss Foundation through the JuBot project.

The authors are with the Institute for Anthropomatics and Robotics, Karlsruhe Institute of Technology, Karlsruhe, Germany, {klas, asfour}@kit.edu

Manuscript received August 18, 2022; revised December 23, 2022; revised March 14, 2023; accepted April 14, 2023.

0000–0000/00$00.00 © 2023 IEEE

Most gearboxes used in robotic actuators have a fixed transmission ratio [3]–[6]. Previous work in constructing our robots ARMAR-6 [7], ARMAR-4 [8] and the KIT-Gripper [9] has shown that it is difficult to achieve human performance in terms of speed, torque, and acceleration with electric motors and fixed transmission ratios. These robots, as well as other humanoid robots like CENTAURO [10], HRP-5P [11] and AILA [12], rely on high gear transmission to reach the torque requirements at the cost of maximum velocity and acceleration. Other robots with a focus on dynamic motions like Spot [13], MIT cheetah [6] or ANYmal [5] on the other hand, use wider flat motors with a lower gear transmission for higher velocities. In these quadruped robots, using two motors with a larger diameter at the beginning of the limb is a reasonable solution. The higher torque region of the dynamic workspace can be temporarily reached by running the motor in its peak operation region. In this operation regime, the motor generates more heat than can be continuously dissipated. The short torque pulses are appropriate for four-legged robots, but difficult for humanoid arms that require long-lasting high torques and sometimes short high-speed bursts. In addition, seven or eight degrees of freedom (DoF) makes it difficult to fit large-diameter motors.

Besides electric actuation with gearboxes, there are artificial muscles that use different physical effects to mimic the behavior and softness of biological muscles. While some variants such as pneumatic muscles are already in industrial use, most of them are still far from actual use in robotic systems in terms of power, durability, and control. As another alternative, hydraulic actuators are available which can be used to drive robots in a space-saving manner [13], [14], but come with their own disadvantages of being sensitive to temperature changes, difficult manufacturing, high cost and danger of leakage. Therefore, we focus on electric actuation in this work.

There are mainly three reasons for the difficulty of achieving human performance by e. g., electric motors, which can achieve higher power densities ($1\,\mathrm{kW/kg}$ [15] to $7\,\mathrm{kW/kg}$ [6]) compared to human muscles ($0.2\,\mathrm{kW/kg}$ [16]). The first reason is strict space and weight constraints with high demands on peak force and speed. Because of space limitations, most robot gearboxes employ a fixed gear ratio. To achieve the maximum speed and torque of a muscle with an actuator with fixed speed and torque limits, an electric motor and a gearbox with much higher peak mechanical power is needed (see Fig. 2). Motors and gearboxes with such high peak power are significantly larger and heavier than the size and weight of the human model [17].

The second reason is that heavy gears in the joint axis require even larger gears for the previous joints in the kinematic chain. With the many DoF needed in humanoid arms, this is a major disadvantage.

The third reason is that electric motors provide their best power densities at high speeds, which makes gearboxes with high transmission ratios R in the range of $R = 10$ to $R = 300$ necessary [3]. Since the motor diameter is a limiting factor in humanoid robot arm design and the necessary torque cannot be directly provided by small motors, it has to be amplified by gearboxes. Their transmission ratio is typically in the range of $R = 100$ for sufficient torque. Since the reflected inertia in gearboxes rises with the power of R, very high reflected inertia in the range of the complete arm weight arises from motor inertia.

The solution we consider in this paper as well as in the subsequent related work is the following: A switchable gearbox to obtain a speed-force profile similar to those of human muscles with high maximum speed and force but low maximum mechanical power (Fig. 2) in a light and linear mechanism to actuate the joints from a position near the body center. Manually or automatically switchable gears offer the advantage of the changeability of transmission ratio but are usually large, heavy, expensive, and complex. Continuously variable transmissions (CVT) allow the adaptation of the force-speed profile. The Uhing rolling ring drive [18] is a linear, friction-based CVT, which converts the rotary movement of a plain shaft into a traversing movement. The transmission ratio is continuously adjustable via the angle between the ring body and the shaft. This adaptation is relatively slow since it is driven by a separate actuator and the mechanism is quite heavy, as it is meant for fixed installations.

Generally, the engineering hybridization principle [19] can inspire interesting designs for combined mechanisms inspired by biology. An idea following this approach with a combination of a joint high-frequency actuator and a base low-frequency actuator [20] elegantly solves the problem of reflected inertia, limited acceleration and inherent safety characteristics necessary for human-centered robotics. They, therefore, combine a strong base actuation for low frequencies and high torques as a series elastic actuator with a light joint actuation for high frequencies and low torques but still need a big and heavy gearbox in the high torque actuator. In the DLR hand arm system [21], [22] several combinations of two motors for variable stiffness actuators are used: Bidirectional antagonistic variable stiffness (BAVS), floating spring joints (FSJ) and antagonistic actuators. The general approach of combining actuators can also be found in hybrid cars or ships with two motors, one for constant mechanical power and one for short peaks. The combination of different specialized actuators can also be found in human muscles, where the three types of slow oxidative (SO), fast oxidative (FO) and fast glycolytic (FG) muscle fibers are combined in each muscle for powerful short and low-power-low-fatigue motions [23].

One solution for a linear mechanism that uses common electric engines as a power source is a mechanism with two motors, in which one drives a nut and the other drives a threaded spindle, as described in [24]. By selecting the motor speeds, the feed rate can be varied over a wide range. Another solution is presented in [25] with a multistage spindle drive for converting a rotary motion into a linear motion with different load-dependent speeds. It consists of telescopically engaged threaded elements of different pitch. The retraction and extension speeds are switched over by frictional force and are adjustable via different friction ratios. In the work [26], a rotary-translation gear unit with a selectable transmission ratio is described. It operates on the principle of the differential spindle, which permits high transmission ratios. The trans-

mission ratio can be changed by switching between normal spindle operation and differential spindle operation. The load-sensitive power transmission device described in [27] uses the alternation between sliding and rolling of a nut on the spindle to change gear stages. The switching is activated by a combination of a brake and a spring.

Limitations to these solutions are a difficult and expensive fabrication of hollow spindles in [25], solid and heavy construction due to large pretension forces in [18] and complexity, as well as limited travel at the high ratio stage in [26]. In [28], the feed rate can be varied over a wide range, but the maximum force of the spindle is limited and, the structure is relatively long. In [27], the position of the nut on the spindle and the switching state of the gearbox cannot be directly controlled or measured. There is a fixed switching point that changes depending on the friction in the brake and requires complex tuning. Not the whole nut runs eccentrically, but only the threaded hole inside the nut is eccentric, whereby only the actuation of the spindle is possible and not also the actuation of the nut.

Important emphases and contributions of this paper are the following. The development of a concept to approach the human force-speed profile with an adaptive shifted transmission and the construction of a compact and light mechanical realization. Furthermore, working prototypes were built and tested in steady and dynamic experiments.

To our best knowledge, no other existing gear mechanism fulfills the requirements for a compact and low-cost, but yet powerful robot with a similar mechanism. The size and weight of existing solutions, along with their lack of specificity for the force-speed profile of muscles, represent the primary drawbacks of those options.

The rest of the article is organized as follows. Section II provides an overview of the requirements for a new mechanism and the concept and kinematic layout of the proposed solution. In Section III, the mechanical design of the ACLD prototype is presented. The prototype is evaluated in Section IV. Section V concludes this article and demonstrates future research prospects.

II. The New Mechanism

A. Requirements

Requirements for a new mechanism are inspired by the mechanical properties of human muscles, but are to be realized on the basis of existing and established mechanical components. The two challenges of strong weight, size, speed, and force requirements and the need for low inertia in the kinematic chain lead to a required compact design and linear actuation as in joints actuated by muscles that are located closer to the body center.

The main inspiration is taken from the force-speed profile of human muscles (Fig. 2) with low maximum power. For the principal shape of the muscle speed-force profile, we chose the *biceps brachii* [2] because of its best-known curve form.We propose a solution with two motors and an automatically switchable gearbox. By combining the power of two drives, the total torque can be increased while taking advantage of the higher speed of the faster mechanism.

A comparison of the approach with human muscles and with a standard solution can be seen in Fig. 2 and 3. In Fig. 2, a $1600\,\mathrm{W}$ motor with fixed transmission ratio is needed. In Fig. 3 the profile is covered with $2 \cdot 200\,\mathrm{W}$ motors with different transmission ratios. If we assume a constant power density of $1\,\mathrm{kW/kg}$ [15] we arrive at $2 \cdot 200\,\mathrm{g}$ instead of $1600\,\mathrm{g}$.

As in human muscles, parts of the requirements are covered by temporary operation, while the simple fallback from temporary operation to either high speed or high force is given. If this is not required, the power-to-weight ratio can be further improved.

The shape of the motor force-speed profile in Fig. 2 and 3 differ, since most gearboxes have fixed limits of speed and torque. Limiting motor power to a triangle is less advantageous, since the gearbox size is unaffected. In Fig. 3 both potential effects are combined, but the usage of rectangular areas would also be feasible.

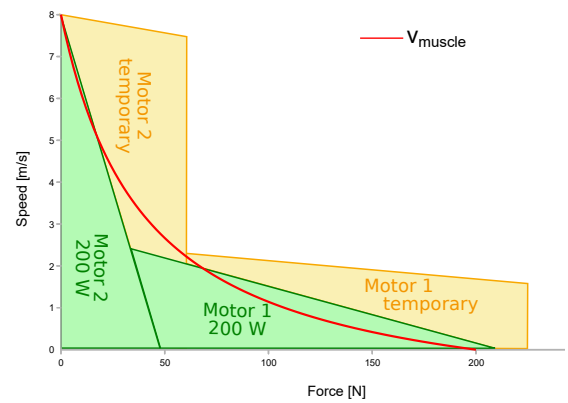

Fig. 3: Force and speed in muscles (biceps brachii from [2]) and **ACLD** concept with 2 gear ratios and triangular motor profiles.

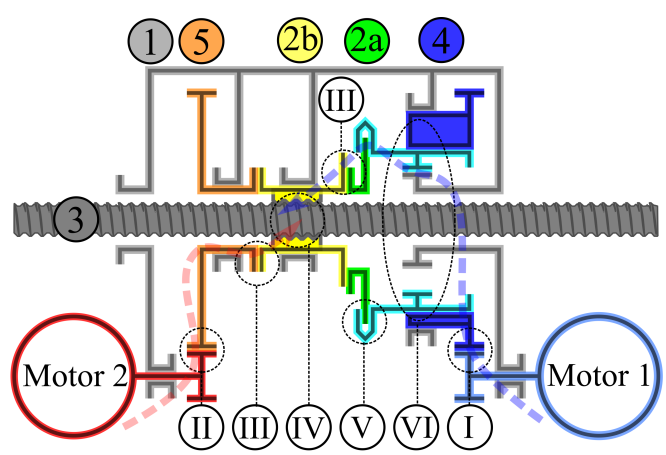

Fig. 4: **Concept and kinematic layout** of the ACLD with actuation I and II, coupling III, linear transmission IV, clutch V and cycloidal drive VI. Power flow of the modes in blue (I) and red (II). The components are marked corresponding to Tab. II.

The three challenges described above are solved in the following way: The speed-force profile with two segments

(Fig. 3) makes adaption to the needs of the specific application possible while the peak mechanical power of both motors and gears are much smaller. This allows the use of much smaller components. The second problem is solved by the linear nature of the drive, which makes it possible to actuate a 2 DoF joint, like the Omniwrist III [29], a compact [30] or a tendon-driven wrist [31] from a position closer the body center leading to a reduction of inertia. Since the torque of both motors driving the two gear stages is added and one has a much lower transmission ratio, the motor and gear stage with the lower transmission ratio can always provide torque for sudden accelerations. This solves the problem of high internal inertia. The proposed solution unifying both gearboxes in a single mechanism with two actuators, is characterized by a small size and a load-dependent automatic selection of the transmission stage.

B. Concept and Kinematic Layout

The solution presented in this paper proposes a two-stage linear drive with automatic and adaptive gear selection, the *Adaptive Cycloidal Linear Drive (ACLD)*. The concept and kinematic layout of the new mechanism is illustrated in Fig. 4

The rotational movement of two actuators I and II is converted into one linear movement in two operation modes which can be used individually and in combination. The two mechanisms for these two operation modes differ in their transmission ratio, with each driven by only one of the two drive sources.

The first actuation I operates a rotary to linear transmission IV, realized by spindle 3 and nut 4 via a clutch V and a cycloidal drive VI. The total transmission ratio results from the thread pitch multiplied by the transmission ratio of the cycloidal gear. This is the first or *Cycloidal Mode*. The clutch has to be preloaded to ensure the functionality of this mode alone.

The second drive source II directly drives the linear transmission IV. The eccentric offset and axial forces are compensated in a coupling III. This is the second operation mechanism: *Spindle Mode*. The transmission ratio is determined only by the thread pitch. The second mechanism is therefore used to implement a small gear ratio (high-speed output), while the first mechanism is used to implement a large gear ratio (low-speed output) that can handle higher forces.

If both drive sources are unning in parallel, this leads to the *Combined Mode*. The combination of the two mechanisms is realized via the clutch V that is activated by the axial load. At low axial forces, the friction in the clutch is low, and the spindle is mainly actuated by the fast *Spindle Mode*. However, depending on the clutch characteristics, the *Cycloidal Mode* can take a part of the load and thus also increase the speed.

With high axial forces, the friction in the clutch is high, and the spindle is actuated by the torque of both the strong *Cycloidal Mode* and the *Spindle Mode*. In between, there is a slight transition based on the clutch characteristics.

The linear speed of the drive spindle 3 is always proportional to the speed of the second motor II. The current transmission ratio can be determined from or set by the speed ratios of both motors.

III. Design of the ACLD Prototype

By combining two stages with two different ratios, a wide range of speed and torque can be achieved.

A prototype with the specifications in Tab. I was built to demonstrate the functionality of the approach.

A. Components of the ACLD

The proposed linear drive with two transmission stages consists of the following components shown in Fig. 5: A housing 1, an eccentric spindle nut 2 consisting of an eccentric element 2a and an internal thread 2b, a cycloidal drive element 4, a spindle drive element 5, eccentric bearings 6, concentric bearings 7 and plain bearing elements 8.

B. Mechanical Realization of the ACLD

The main difference between the idea (Fig. 4) and its mechanical realization (Fig. 5) in the prototype is the unification of the linear transmission IV, the clutch V and the cycloidal drive VI in one mechanism. It provides two modes, the *Cycloidal Mode* and the *Spindle Mode*.

In both modes the spindle 3 can move linearly along a center axis, guided by plain bearing elements 6 in the housing 1. The rotation of the eccentric spindle nut 2 determines the axial position of the spindle. The rotational movement of the spindle must be prevented separately.

In *Cycloidal Mode* the cycloidal drive element 4 is driven by the first motor (blue) I. This mode is characterized by a geared actuation of the spindle, an indirect actuation of the second motor (red), and a rolling contact between spindle and nut without tangential sliding (Fig. 6a). The rotary axis of the eccentric spindle nut rotates around the center axis.

The rotatability of the cycloidal drive element 4 relative to the spindle also changes the orientation of the eccentricity of the cycloidal drive element 4 relative to the spindle and thus the contact point between the spindle and eccentric spindle nut 2. This results in cycloidal drive VI like rolling motion of the eccentric spindle nut on the spindle.

In *Spindle Mode* the eccentric spindle nut 2 is driven by the second motor (red) II via the spindle drive element 5. This mode is characterized by direct actuation of the spindle, thus providing high speed, and sliding contact between the spindle and the nut (Fig. 6b). The rotation axis of the eccentric spindle nut is fixed. The coupling III compensates for offset and decouples axial forces.

In both modes the interaction of nut 2 and spindle 3 realizes a rotary to linear transmission IV. The friction between spindle 3 and nut 2 depends on the axial load. This realizes the functionality of a clutch V controllable by axial force. Thus, the contribution of both modes is controlled by the

Weight	100 g
Diameter	45 mm
Speed	225 mm/s
Payload	480 N
Power (Speed x Payload)	108 W

TABLE I: Specifications of the ACLD prototype

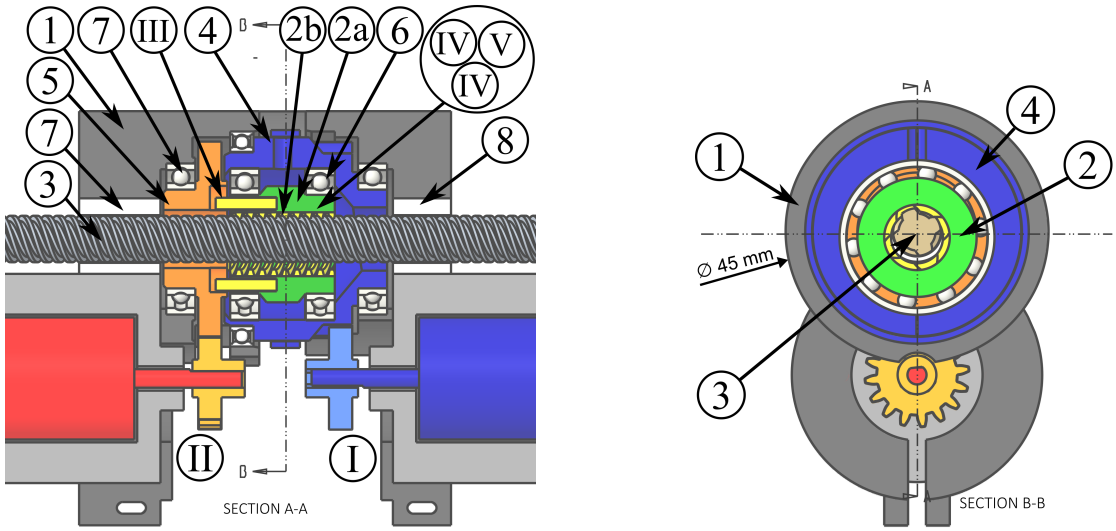

Fig. 5: **Mechanical realization** of the ACLD.
Sectional drawing A-A (Left) and B-B (Right).

Components	
1	Housing
2	Eccentric spindle nut
2a	Eccentric element
2b	Spindle nut
3	Spindle
4	Cycloidal drive element
5	Spindle drive element
6	Eccentric bearings
7	Concentric bearings
8	Plain bearings
	Functionality
I	First (cycloidal) actuation (blue)
II	Second (spindle) actuation (red)
III	Coupling with force decoupling
IV	Rotary to linear transmission
V	Clutch with offset compensation
VI	Cycloidal drive

TABLE II: Essential components of the ACLD

axial force. Through the functionality of a linear transmission IV, a clutch V and a cycloidal drive VI is realized in one mechanism.

In the experimental results, we find that these modes are not completely separate with a sudden shift but have a slight transition (Fig. 12). As a result, the cycloidal stage increases the force even at high speeds by reducing the load on the spindle drive. The self-locking of the nut prevents the motor from being driven back. If the pitch and thus the friction force is selected below self-locking but the remaining force below the driving force of the spindle motor, the mechanism can be back-drivable.

The threads of the drive spindle and drive element have the same pitch ($1.5\,\mathrm{mm}$) and the internal thread diameter of the drive element ($10\,\mathrm{mm}$) is bigger than the external thread diameter of the drive spindle ($8\,\mathrm{mm}$).

The spindle transmission ratio R_S and the cycloidal ratio R_C can be selected as follows: R_S at reduced friction compared to a pure spindle drive determines the maximum speed and R_C the maximum transmission ratio between both motors (Fig. 12). Future mathematical modeling will be required for a more detailed dynamic analysis.

The cycloidal transmission ratio R_C is calculated from the effective thread diameters of the drive element D and the drive spindle d, R_S from the spindle pitch p:

$$R_C = D/(D-d) \tag{1}$$

$$R_S = \frac{2 \cdot \pi}{p} \tag{2}$$

The spindle 3 and the nut 2 engage with each other over several tooth flanks and are thus suitable for transmitting high axial force to the drive spindle.

The second drive source has an overload protection with an electrical power limitation or a cut-off. The two motors are coupled to the hollow shaft 2 and the drive element 2, respectively, via gear drives. The nut in these experiments was 3D-printed from PLA and lubricated with PTFE spray.

C. Variants

In the prototype, the necessary limitation of the spindle rotation must be ensured by the following joint. In one possible variant, the anti-rotation device between the drive spindle and housing is realized directly in the gear unit by means of corresponding guides.

Another variant of the linear actuator is that the drive element consists of several coupled, eccentric nuts whose contact surface is on opposite sides of the spindle. The use of several coupled nuts eliminates the need for separate guidance of the drive spindle in plain bearings. Friction in these plain bearings is eliminated.

For easy production, the spindle is preferably realized with a standard thread, e. g., trapezoidal thread. With suitable drive elements/nuts (e. g., 3D printed), there is a large contact area

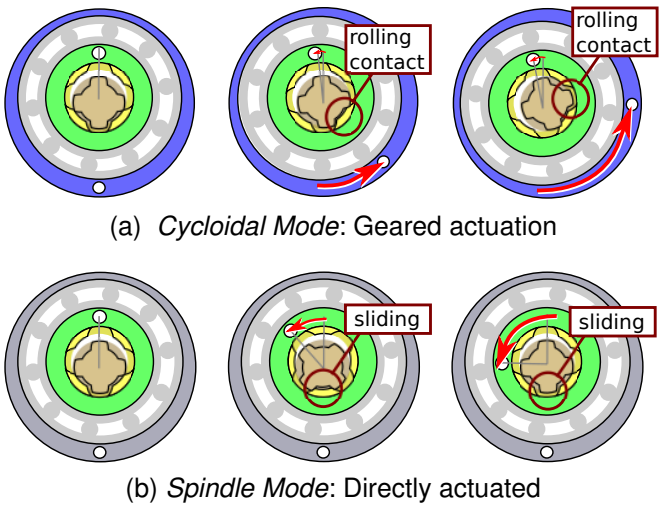

Fig. 6: Motion of the drive components in *Cycloidal* and *Spindle Mode*.

and no overlaps during the movement. Alternatively, the drive element/nuts can be designed with a standard thread and the spindle with a thread adapted to it.

D. Friction

When the hollow shaft is driven by the first drive source (*Cycloidal Mode*), the friction losses are lower, since the nut is mainly rolling on the spindle and only sliding two thread heights during one rotation. During one rotation of the spindle nut. a point on the thread moves outward and inward by one threat height. When the drive element is driven directly via the second drive source (*Spindle Mode*), the friction losses are significantly higher, since the nut is sliding on along the complete spindle diameter during one rotation, but the transmitted axial forces are also lower. The motions of the parts in both modes can be also seen in Fig. 6. The frictional power losses can be approximately calculated by:

$$P_{loss_{cycloidal}} = 2 \cdot h \cdot \nu \cdot \mu \cdot F_{ax} \tag{3}$$

$$P_{loss_{spindle}} = \pi d \cdot \nu \cdot \mu \cdot F_{ax} \tag{4}$$

where

h	is the tooth height
d	is the spindle diameter
ν	is the is rotational frequency
μ	is the friction coefficient
F_{ax}	is the axial force on the spindle.

E. Actuation

The gear mechanism in the prototype experiments is actuated by two DC motors [32] with a rated power of 20 W via a 2:1 spur gear. The motor characteristics of both motors from the evaluation experiment were measured (Fig. 7) for output torque estimation. The drive sources can be various electrical DC or EC motors without or with gears. Depending on the motor type and control details, the second drive source has

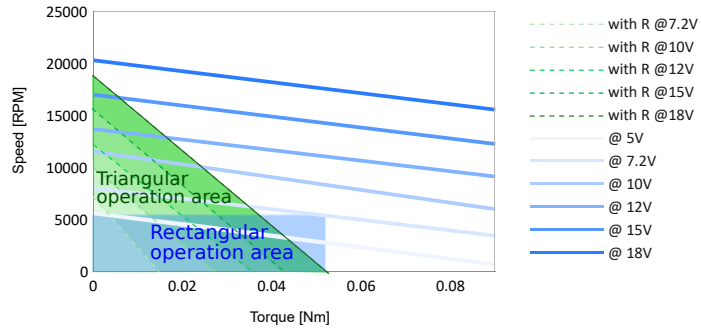

Fig. 7: Measured performance profile of motor 1 in the experimental setup. Rectangular operation area is limited by motor heat, gearbox speed limit and gearbox torque limit. Triangular operation area is limited by series resistance. Unlimited profiles with stall currents destroying motor and gear at higher voltages - similar to most EC/DC motors.

an overload protection with a current limitation to prevent overheating of this motor at high loads. as described in Sec. III-F.

For simplicity of control, the linear current-to-torque relationship in the prototype was realized with DC motors and analog linear current limitations (Sec. III-F). A prototype using stepper motors (see Fig. 1) was built in addition to DC motor prototypes for high torque tests and exact speed relations between both motors. Due to the heavy weight of the stepper motors, this is not the ideal solution for humanoid robots, but suitable for a single robot arm with actuation from the fixed base.

In the prototype, both DC motors are controlled jointly by means of voltage or current control. In the case of stepper motors, the speeds for both motors are preferably set according to the ratio of the cycloidal transmission in Fig. 12 or to the desired transmission ratios.

F. Electronics

If the speed (proportional to voltage and torque) and torque (proportional to current) are not limited by fixed values but depend on the maximum electrical power, the thermal load on the motor and gears can be reduced to reach higher speeds. This can be used additionally to the mechanical characteristics of the ACLD to reduce motor size. This is similarly proposed in [6] where the authors state that "The recommended voltage is set concerning the thermal failure in the case that users command voltage without the knowledge of the coil temperature. [...] Within the continuous current limit, the motor can generate much higher power than the rating provided by the manufacturer with a fixed voltage limit." In addition to the continuous current limitation, the increasing current limit reduces maximum power and thus thermal load on the drive. which makes higher top speeds of the spindle nut possible. This is called triangular operation area and is compared to the rectangular operation area for the motors used in the prototype in Fig. 7. In the prototype, a linear function between maximum speed and maximum torque is achieved by a series resistance (chosen to limit the current at stall to a tolerable level) and the

voltage of the motors (rated voltage of 7.2 V) can be increased to 30 V resulting in a much higher speed without destroying the motor by electrical or the gear by frictional overheating. As can be seen in the figure, the current limitation on the prototype is set to achieve the maximum continuous torque at 18 V. Without the current limitation, the maximum torque is exceeded at this voltage and the motor overheats rapidly, but even at nominal voltage, the motor would overheat within seconds at stall.

Both the electric motor and the spindle can handle short overloads due to thermal inertia. which could be exploited in a more sophisticated control scheme.

G. Sensing

The speed in prototype experiments was measured with commutator peaks in the recorded motor current [33] and a digital tachometer. Force was measured with calibrated weights as loads and a strain gauge force sensor.

In a robotic application, the gear can be easily equipped with several sensors for feedback and control. All motors can include relative encoders that allow precise velocity and position control. and a simple force sensor can measure the axial load and thus the torque in the robot joint. Absolute encoders are preferably included in the actuated joint.

H. Costs

The linear actuator is advantageously characterized by a simple design with a high proportion of standard components (bearings, drive spindle, motors, etc.). The remaining components, such as the drive element, the hollow shaft or plain bearings, can be manufactured from friction-optimized plastic by simple means, such as 3D printing, since the accuracy requirements are relatively low. Due to the large surfaces available for force transmission, high forces comparable to spindle drives with nuts made of tribological plastics are possible. This is very beneficial for the production of customized, cost-effective, and lightweight linear drives with multiple transmission ratios.

In the design, the parts to be manufactured individually, in particular the housing, the hollow shaft, plain bearing elements, and the drive element, can be produced predominantly without support material in FDM 3D printing. This makes this design particularly suitable for inexpensive and adaptable production in different sizes and gear ratios.

IV. Experimental Evaluation

To evaluate the proposed gear design, we measure important parameters like the speed-torque profiles in a prototype and compare the prototype with state-of-the-art solutions for robotic applications.

A. Speed-Torque Profile

To evaluate whether the theoretical speed-force profile is achieved by the prototype, the curve was obtained by several experiments at different loads (see Fig. 8). As expected. the resulting force is mainly a sum of the separate torques

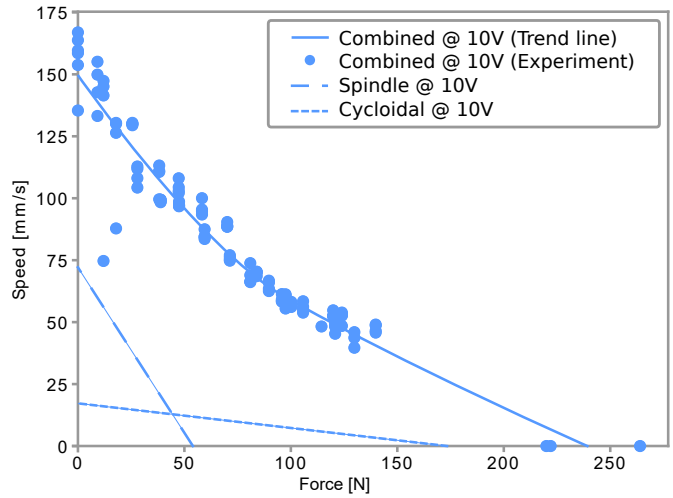

Fig. 8: Steady state force-speed profiles of the prototype @ 10V with spindle and cycloidal mechanism separate and combined. In the *Combined Mode*. the forces of both mechanisms are added and efficiency is improved.

with some losses at higher forces. The resulting speed also surpasses the speeds of the separate mechanisms. The reason for the increased speed is probably caused by two effects: The lower friction in *Combined Mode* compared to *Spindle Mode* (Tab. IV) and the slow transition in the transmission ratio when moving from low to high forces (Fig. 12) whereby the cyclodial stage can support the spindle stage also at high speeds.

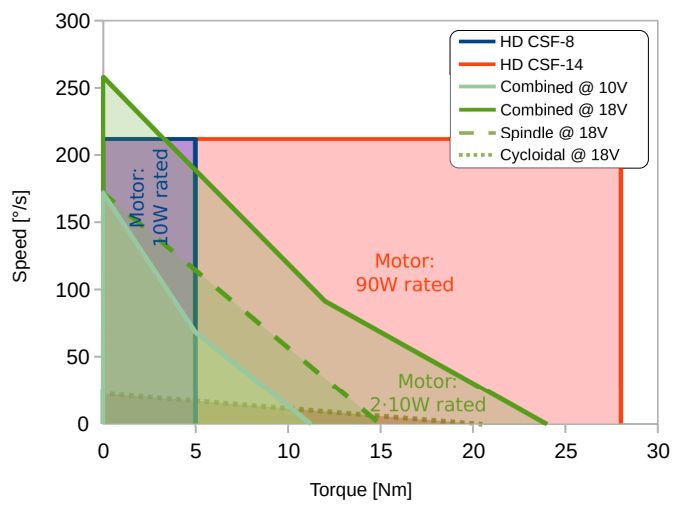

Fig. 9: Torque and speed of the prototype at different voltages and with spindle and cycloidal mechanism separate and combined. Harmonic Drive CSF-8-100 and CSF-14-100 with Maxon RE 25 (10W) and RE 35 (90W) Motors for comparison. Detailed values in Tab. V

.

B. Dynamic properties

The dynamic properties are evaluated in an experimental setup comparable to a drive actuating a wrist with inertia

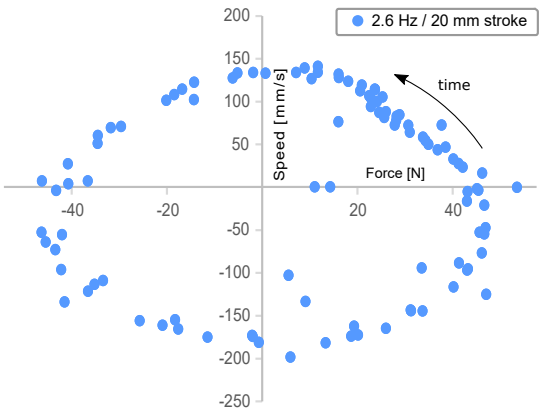

Fig. 10: Dynamic force and speed curve of the prototype in oscillating motion. The experimental setup is comparable to a drive actuating a wrist with a tennis racquet in terms of load ($0.017\,\mathrm{kg\,m^2}$), amplitude ($40°$) and obtained velocities ($300\,°/\mathrm{s}$).

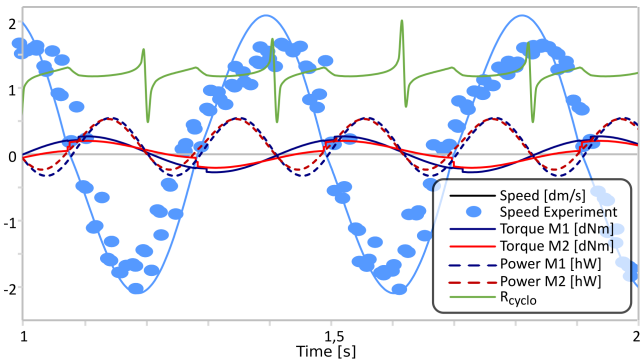

Fig. 11: Time-series data of the prototype in oscillation motion. The speed is measured in the experiment. The other parameters are calculated from motor parameters, inertia of the components and a constant friction force. Different inertias of the stages cause peaks in R_{cyclo} (cycloidal transmission ratio).

similar to a hand with a light tennis racquet ($0.5\,\mathrm{kg}$ bar with $0.32\,\mathrm{m}$ length). The bar is actuated with a lever of $32\,\mathrm{mm}$, moves with an amplitude of $40°$ and reaches a peak speed of $300\,°/\mathrm{s}$. This is comparable to forehand wrist speed performed by skilled tennis players [34]. Time-series data of this experiment is shown in Fig. 11. The velocity is measured in the experiment, the other parameters are calculated using a Matlab Simulink model, where the friction parameters are chosen to match the results of the static and dynamic experiments.

C. Transmission Ratios

Due to the frictional character of the cycloidal drive stage, the transmission ratio of this second mechanism is not exactly fixed. but depends on the effective rolling radii of the nut on the spindle and slip.

A spindle diameter between $6.2\,\mathrm{mm}$ and $8\,\mathrm{mm}$ and a nut diameter between $8.7\,\mathrm{mm}$ and $10\,\mathrm{mm}$ lead to a possible transmission ratio between 4.5 and 12.5 (see eq. 1). The measured transmission ratio of only the cycloidal drive stage is between 6.3 and 7.2 in the experiments. This means that the

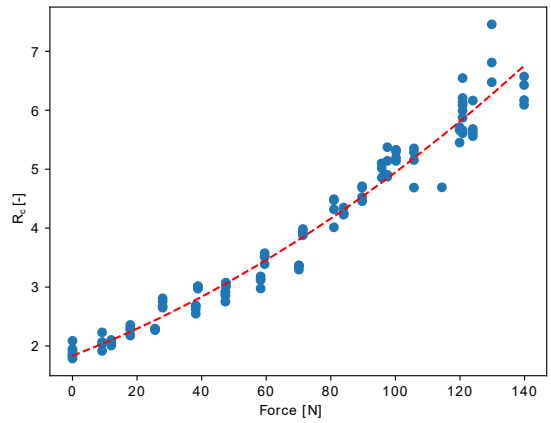

Fig. 12: Transmission ratio R_c of the cycloidal part of the **ACLD** corresponding to the $10\,\mathrm{V}$ force-speed profile. Fitted curve in red.

rolling contact is approximately in the middle of the thread, slightly closer to the outer diameter.

As displayed in Fig. 12 in the *Combined Mode*. the transmission ratio of the cycloidal part of the ACLD rises slowly from 2 to 7 for rising forces. This is a beneficial behavior leading to higher speeds. Additionally, this slow transition is better for control compared to a sudden transmission ratio change.

D. Efficiency

Since friction forces are an important aspect when considering efficiency, we first examined them. To calculate friction in the different switching states. we performed several experiments at different voltages at stall torque and no-load speed as well with both motors, the first motor or the second motor driven. We measured both motor performance curves first and then calculated the theoretical force without friction from motor current and compare it to the measured force. It was assumed that the difference corresponds to the frictional forces. These are given for different modes in Tab. III. In Tab. IV the output forces at stall are related to the maximum theoretical forces based on motor current. Since friction forces are partly constant. the efficiency should rise at higher loads. The force conversion efficiency of the spindle increases dramatically when both mechanisms are active.

To analyze the efficiency of our ACLD prototype. we calculated the efficiency for the data points from the $10\,\mathrm{V}$ steady state force and speed curve. The efficiency was calculated from the motor's mechanical power output based on current and motor speed. and the output power of the drive based on measured speed and force.

For comparison, we added the efficiency data of the Harmonic Drive CSF-14-100-2XH-F. Since the efficiency depends on many parameters, the temperature was fixed to $20\,°\mathrm{C}$ and the varying speed at a given voltage compared to the efficiency at different speeds given by Harmonic Drive. The efficiency of the Harmonic Drive CSF-14-100 [35] at room temperature is between 70% and 22% and thus comparable to the efficiency of the ACLD. A detailed comparison of the ACLD and Harmonic Drive efficiency curves is shown in

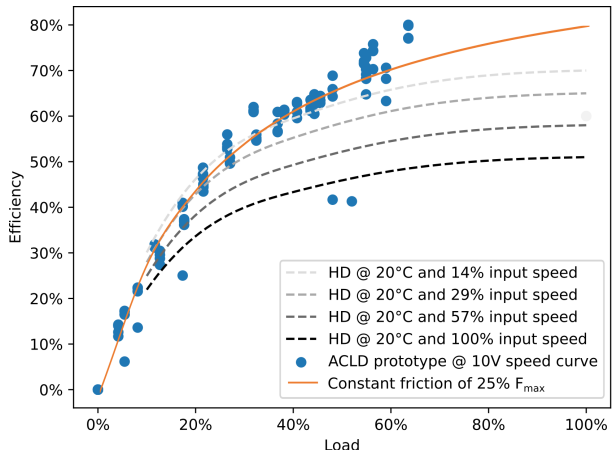

Fig. 13: Steady state efficiencies of the ACLD prototype at 10V speed curve and the Harmonic Drive CSF-14-100-2XH-F at different speeds and 20°C. The efficiency can be well estimated with a constant friction force.

Mode	Output	Spindle Fric.	Cycloidal Fric.
Combined	Stall (220N)	72N	72N
Combined	No load speed	73N	67N
Spindle	Stall (54N)	123N	-
Spindle	No Load speed	125N	-
Cycloid	Stall (173N)	-	11N
Cycloid	No Load speed	-	92N

TABLE III: Absolute Friction Values @ 10Vcalculated from measured forces and max. theoretical forces from motor current and spindle transmission.

Voltage	Mode	Force efficiency
7.2V	Combined	58.1%
7.2V	Spindle	36.4%
7.2V	Cycloid	78.1%
10V	Combined	60.4%
10V	Spindle	35.6%
10V	Cycloid	93.8%
12V	Combined	60.0%
12V	Spindle	40.0%
12V	Cycloid	97.9%

TABLE IV: Force efficiency at stall as ratio of measured forces to max. theoretical forces from motor current and spindle transmission.

Fig. 13. As can be seen in the plot, the efficiency can be well described with a constant friction force of 25% of the maximum force and thus the following formula:

$$\eta_{est} = \frac{F_{out} \cdot v}{F_{in} \cdot v} = \frac{F_{out}}{(F_{out} + 0.25 \cdot F_{max})} \tag{5}$$

E. Comparison to the state-of-the-art

As Harmonic Drives are the state-of-the-art in robotics both in research and industry (Panda [36], UR5 and UR10 [37]) we compare the ACLD with Harmonic Drive CSF [35] gear units.

Due to its small size, the wrist is one of the most difficult joints in humanoid robots, so a 2 DoF wrist was chosen for comparison. It requires tight integration of both motors and needs to be both forceful for holding and fast in the pre-grasp phase. To compare the linear motion of the ACLD with the rotary motion of a Harmonic Drive, the following setting was chosen: The two Harmonic Drives actuate the joints directly in the joint axis while the ACLD actuates a 2 DoF joint mechanism (e. g., [29], [30], [38]) with an effective lever arm of $50\,\mathrm{mm}$. In Table V the results are presented. The *power area* in this table is the product of speed and strength limits - the maximum mechanical power that an actuator with fixed speed and force or torque limits would require to cover the same area.

Gearbox	CSF-8-100-2XH-F [35]	CSF-14-100-2XH-F [35]	Prototype (lever 50 mm)
Size	⌀43 mm	⌀73 mm	⌀45 mm
Length	31 mm	45 mm	58 mm
Power area[1]	18 W	102 W	108 W
Weight	100 g	295 g	118 g+3 g/cm
Max. speed	212 °/s	212 °/s	258 °/s
Torque	5 N m	28 N m	24 N m
Gear inertia	3 kg mm^2	33 kg mm^2	①: 4.0 kg mm^2 ②: 1.3 kg mm^2
Trans. ratio	100	100	①: $209 \cdot R_c$ ②: 209
Example motor	RE 25 [39]	RE 35 [39]	2 · RE 25 [39]
Peak power	36 W	204 W	2· 32 W
Rated power	10 W	90 W	2· 10 W
Rotor inertia	1 kg mm^2	7 kg mm^2	1.0 kg mm^2
Refl. inertia	40 g m^2	400 g m^2	①:240 g m$^2 \cdot R_c^2$ ②: 80 g m^2
1) Limits: $\omega \cdot \tau$, $F \cdot v$	4.8 Nm · 3500 RPM	28Nm · 3500 RPM	480 N · 225 mm/s

TABLE V: Comparison of the ACLD with Harmonic Drives

To compare the capabilities of the prototype from Tab. V to the muscles which drive the human wrist, we use the following numbers: A maximum torque of between $3\,\mathrm{N\,m}$ and $20\,\mathrm{N\,m}$ [40], depending on the individual and wrist position and a maximum speed between $2\,\mathrm{rad/s}$ and $7\,\mathrm{rad/s}$ for a typical individual [41] depending on motion direction. With these figures, we see that the maximum torque of the wrist driven by the prototype of $24\,\mathrm{N\,m}$ and the speed of about $9\,\mathrm{rad/s}$ are in the top range of the human ones. A robot arm built with actuators similar to the prototype would have a diameter of at least $2{\cdot}45\,\mathrm{mm}$, making them thicker than their human counterparts, however still suitable for humanoid robots.

F. Limitations

A major limitation of the presented mechanism is that two motors are needed. These two motors are much lighter and smaller than one motor covering the entire scale (see Sec. III-E), but the additional control electronics add cost and require space.

The mechanism only works for linear actuation. There is no similar solution for rotary actuation yet. Linear actuation has advantages and disadvantages that have to be balanced.

If muscle-type force-speed profiles are not required, but the full range of maximum speed and maximum force is to be used, other drive mechanisms are preferable.

V. Conclusion

The ACLD, which can be used in applications where muscle-like force-velocity curves are advantageous, was presented. A prototype was built to demonstrate that this new linear gear can be superior to conventional motor-gearbox combinations in some applications.Data from dynamic experiments indicate that a humanoid robot with human agility and power for some motions is possible with this drive, while the live-time and different versions and sizes of the mechanism still have to be tested.

By selection of spindle pitch and cycloidal transmission, the drive can be adapted to the required curves. Since the required speed-force curves are only available for a few joints, curves for all joints have to be derived from recorded human motion with known loads. Incorporating mathematical modeling of the ACLD into the design process may enable us to optimize the performance of the system to the specific requirements. This mathematical model could also give more insight into the dynamics of the switching process.

For different applications, the arrangement of the components can be changed for different versions: On-axis motors, one motor, and a clutch or multiple displaced drive elements, which makes the sliding bearings unnecessary. These versions are not explained here in detail and still need to be tested in a prototype. As the next step, we plan to develop prototypes in a size suitable for humanoid elbow and shoulder joints, considering human speeds, torques, sizes, and weights.

Overall, we investigated the ability of the Adaptive Cycloidal Linear Drive to reproduce the torque-velocity profiles of human muscles. We provided experimental data to better understand the capabilities of this system and showed that it can be advantageous in some applications with the need for these profiles.

References

[1] J. Alcazar, R. Csapo, I. Ara, and L. M. Alegre, "On the shape of the force-velocity relationship in skeletal muscles: The linear, the hyperbolic, and the double-hyperbolic," *Frontiers in Physiology*, vol. 10, p. 769, 2019.

[2] D. Wilkie, "The relation between force and velocity in human muscle," *The Journal of Physiology*, vol. 110, no. 3-4, pp. 249–280, 1949.

[3] H. Matsuki, K. Nagano, and Y. Fujimoto, "Bilateral drive gear—a highly backdrivable reduction gearbox for robotic actuators," *IEEE/ASME Transactions on Mechatronics*, vol. 24, no. 6, pp. 2661–2673, 2019.

[4] S. Rader, L. Kaul, P. Weiner, and T. Asfour, "Highly integrated sensor-actuator-controller units for modular robot design," in *IEEE International Conference on Advanced Intelligent Mechatronics (AIM)*, 2017, pp. 1160–1166.

[5] M. Hutter, C. Gehring, A. Lauber, F. Gunther, C. D. Bellicoso, V. Tsounis, P. Fankhauser, R. Diethelm, S. Bachmann, M. Blösch *et al.*, "Anymal-toward legged robots for harsh environments," *Advanced Robotics*, vol. 31, no. 17, pp. 918–931, 2017.

[6] S. Seok, A. Wang, D. Otten, and S. Kim, "Actuator design for high force proprioceptive control in fast legged locomotion," in *2012 IEEE/RSJ International Conference on Intelligent Robots and Systems*. IEEE, 2012, pp. 1970–1975.

[7] T. Asfour, M. Waechter, L. Kaul, S. Rader, P. Weiner, S. Ottenhaus, R. Grimm, Y. Zhou, M. Grotz, and F. Paus, "Armar-6: A high-performance humanoid for human-robot collaboration in real-world scenarios," *IEEE Robotics & Automation Magazine*, vol. 26, no. 4, pp. 108–121, 2019.

[8] T. Asfour, J. Schill, H. Peters, C. Klas, J. Bücker, C. Sander, S. Schulz, A. Kargov, T. Werner, and V. Bartenbach, "Armar-4: A 63 dof torque controlled humanoid robot," in *2013 13th IEEE-RAS International Conference on Humanoid Robots (Humanoids)*. IEEE, 2013, pp. 390–396.

[9] C. Klas, F. Hundhausen, J. Gao, C. R. Dreher, S. Reither, Y. Zhou, and T. Asfour, "The kit gripper: A multi-functional gripper for disassembly tasks," in *2021 IEEE International Conference on Robotics and Automation (ICRA)*. IEEE, 2021, pp. 715–721.

[10] L. Baccelliere, N. Kashiri, L. Muratore, A. Laurenzi, M. Kamedula, A. Margan, S. Cordasco, J. Malzahn, and N. G. Tsagarakis, "Development of a human size and strength compliant bi-manual platform for realistic heavy manipulation tasks," in *2017 IEEE/RSJ International Conference on Intelligent Robots and Systems (IROS)*. IEEE, 2017, pp. 5594–5601.

[11] K. Kaneko, H. Kaminaga, T. Sakaguchi, S. Kajita, M. Morisawa, I. Kumagai, and F. Kanehiro, "Humanoid robot hrp-5p: An electrically actuated humanoid robot with high-power and wide-range joints," *IEEE Robotics and Automation Letters*, vol. 4, no. 2, pp. 1431–1438, 2019.

[12] J. Lemburg, J. de Gea Fernández, M. Eich, D. Mronga, P. Kampmann, A. Vogt, A. Aggarwal, Y. Shi, and F. Kirchner, "Aila-design of an autonomous mobile dual-arm robot," in *2011 IEEE International Conference on Robotics and Automation*. IEEE, 2011, pp. 5147–5153.

[13] E. Guizzo, "By leaps and bounds: An exclusive look at how boston dynamics is redefining robot agility," *IEEE Spectrum*, vol. 56, no. 12, pp. 34–39, 2019.

[14] S.-H. Hyon, D. Suewaka, Y. Torii, and N. Oku, "Design and experimental evaluation of a fast torque-controlled hydraulic humanoid robot," *IEEE/ASME Transactions on Mechatronics*, vol. 22, no. 2, pp. 623–634, 2016.

[15] Y. Tanaka, S. Sakama, K. Nakano, and H. Kosodo, "Comparative study on dynamic characteristics of hydraulic, pneumatic and electric motors," in *Fluid Power Systems Technology*, vol. 56086. American Society of Mechanical Engineers, 2013, p. V001T01A037.

[16] I. W. Hunter and S. Lafontaine, "A comparison of muscle with artificial actuators," in *Technical Digest IEEE Solid-State Sensor and Actuator Workshop*. IEEE, 1992, pp. 178–185.

[17] D. A. Winter, *Biomechanics and motor control of human movement*. John Wiley & Sons, 2009.

[18] J. Uhing, "Rolling ring drive for converting a rotary movement into a feed movement," DE Patent DE1 210 647B, Feb., 1966.

[19] W. J. Zhang, P. R. Ouyang, and Z. H. Sun, "A novel hybridization design principle for intelligent mechatronics systems," in *The Abstracts of the international conference on advanced mechatronics: Toward evolutionary fusion of IT and mechatronics: ICAM 2010.5*. The Japan Society of Mechanical Engineers, 2010, pp. 67–74.

[20] M. Zinn, B. Roth, O. Khatib, and J. K. Salisbury, "A new actuation approach for human friendly robot design," *The International Journal of Robotics Research*, vol. 23, no. 4-5, pp. 379–398, 2004.

[21] M. Grebenstein, A. Albu-Schäffer, T. Bahls, M. Chalon, O. Eiberger, W. Friedl, R. Gruber, S. Haddadin, U. Hagn, R. Haslinger *et al.*, "The dlr hand arm system," in *2011 IEEE International Conference on Robotics and Automation*. IEEE, 2011, pp. 3175–3182.

[22] W. Friedl, H. Höppner, F. Petit, and G. Hirzinger, "Wrist and forearm rotation of the dlr hand arm system: Mechanical design, shape analysis and experimental validation," in *2011 IEEE/RSJ International Conference on Intelligent Robots and Systems*. IEEE, 2011, pp. 1836–1842.

[23] J. G. Betts, J. Wise, K. A. Young, P. Desaix, E. Johnson, J. E. Johnson, O. Korol, D. Kruse, B. Poe, and M. D. Womble, *Anatomy and Physiology*. Acton, MA, Houston, Texas: XanEdu ; OpenStax College, Rice University, 2017, oCLC: 1083766492.

[24] H. Fickler, "Linear drive device with two engines," DD Patent DD211 768A5, Jul., 1984.

[25] K. Kober and A. Rampp, "Multistage spindle drive for converting rotary motion into linear motion," EP Patent EP0 776 285B1, Jun., 1998.

[26] M. Brand, "Rotation-translation gearbox with shiftable transmission," DE Patent DE102 013 015 257B3, Mar., 2015.

[27] H. T. Minbuta and M. T. Sotome, "Load-sensitive drive power transmission device," DE Patent DE102 007 059 457A1, Jun., 2008.

[28] H. Fickler, "Linear drive device with two motors," CH Patent CH647 306A5, Jan., 1985.

[29] J. Sofka, V. Skormin, V. Nikulin, and D. Nicholson, "Omni-wrist III-a new generation of pointing devices. part i. laser beam steering devices-mathematical modeling," *IEEE Transactions on Aerospace and Electronic Systems*, vol. 42, no. 2, pp. 718–725, 2006.

[30] C. Klas and T. Asfour, "A compact, lightweight and singularity-free wrist joint mechanism for humanoid robots," in *IEEE/RSJ International Conference on Intelligent Robots and Systems (IROS)*, 2022, pp. 0–0.
[31] A. Toedtheide, J. Kühn, E. P. Fortunić, and S. Haddadin, "An integrated, force-sensitive, impedance controlled, tendon-driven wrist: Design, modeling, and control," in *2020 IEEE-RAS 20th International Conference on Humanoid Robots (Humanoids)*. IEEE, 2021, pp. 25–32.
[32] "RC4WD-540." [Online]. Available: https://tamico.de/RC4WD-540-Crawler-Brushed-Motor-55T
[33] E. Vazquez-Sanchez, J. Sottile, and J. Gomez-Gil, "A novel method for sensorless speed detection of brushed dc motors," *Applied Sciences*, vol. 7, no. 1, p. 14, 2017.
[34] S. R. Loushin, S. Kakar, S. U. Tetzloff, P. Lubbers, T. S. Ellenbecker, and K. R. Kaufman, "Upper extremity kinematics and electromyographic activity in uninjured tennis players," *Applied Sciences*, vol. 12, no. 9, p. 4638, 2022.
[35] *Speed Reducers for Precision Motion Control, Reducer Catalog, Gear Units CSF Mini*, Harmonic Drive LLC, September 2019, rev 20190919.
[36] *Panda Datasheet*, Franka Emika, May 2019.
[37] *Robotic and Automation*, Harmonic Drive AG, June 2016.
[38] K. Choi, J. Kwon, T. Lee, C. Park, J. Pyo, C. Lee, S. Lee, I. Kim, S. Seok, Y.-J. Kim *et al.*, "A hybrid dynamic model for the ambidex tendon-driven manipulator," *Mechatronics*, vol. 69, p. 102398, 2020.
[39] *Product Range 2022/23*, Maxon Precicion Drive Systems, 2022.
[40] Y. Yoshii, H. Yuine, O. Kazuki, W.-l. Tung, and T. Ishii, "Measurement of wrist flexion and extension torques in different forearm positions," *Biomedical engineering online*, vol. 14, no. 1, pp. 1–10, 2015.
[41] D. C. Flores, S. Laurendeau, N. Teasdale, and M. Simoneau, "Quantifying forearm and wrist joint power during unconstrained movements in healthy individuals," *Journal of NeuroEngineering and Rehabilitation*, vol. 11, no. 1, pp. 1–7, 2014.

Cornelius Klas Cornelius received his degree as Dipl.-Ing. in Mechanical Engineering at KIT in 2012 and worked on the design of the humanoid robot ARMAR-4 during his studies. In 2018, he returned to work on humanoid and disassembly robots. He is currently a research scientist and PhD student at the Institute of Anthropomatics and Robotics, the High Performance Humanoid Technologies Lab (H^2T). His research interests are in the development and design of humanoid robots and robotic grippers.

Tamim Asfour is full Professor at the Institute for Anthropomatics and Robotics, where he holds the chair of Humanoid Robotics Systems and is head of the High Performance Humanoid Technologies Lab (H^2T). His research interest is 24/7 humanoid robotics. Specifically, he studies the mechano-informatics of humanoids as the synergetic integration of informatics, artificial intelligence, and mechatronics into complete humanoid robot systems, which are able to perform versatile tasks real world. He is the developer and the leader of the development team of the ARMAR humanoid robot family.